PERGAMON

International Journal of Heat and Mass Transfer 44 (2001) 3907–3917

International Journal of HEAT and MASS TRANSFER

www.elsevier.com/locate/ijhmt

Integrative thermodynamic optimization of the environmental control system of an aircraft

Jose V.C. Vargas, Adrian Bejan *

Department of Mechanical Engineering and Materials Science, School of Engineering, Box 90300, Duke University, Durham, NC 27708-0300, USA

Received 18 August 2000; received in revised form 20 December 2000

Abstract

In this paper we propose to optimize the geometric configuration of a component by maximizing the global thermodynamic performance of the much larger system that contains the component. This "integrative" approach departs from current thermodynamic optimization practice in which the configuration of a component (e.g., heat exchanger) is optimized by itself, in isolation. In the present example the larger system is an aircraft and the component is its environmental control system (ECS). We show that the configuration of the ECS impacts the performance (exergy destruction, fuel consumption) of the aircraft in two ways, not one: through its own irreversibility, and its weight-related contribution to the power required to sustain the flight. By minimizing the thermodynamic losses at the aircraft level, we deduce all the geometric details of the cross-flow heat exchanger that dominates the weight and structure of the ECS. The optimized geometry is robust with respect to changes in some of the operating parameters that have to be specified. The integrative method illustrated in this paper is generally applicable to the optimization of architecture in other systems where all the functions are driven by the exergy of the fuel installed onboard.

1. Integrative thermodynamic optimization

In this paper we explore the basis for an integrative approach to the conceptual design of energy systems for aircraft. The integrative design philosophy means that an entire system can be conceived from the beginning as a construct designed to perform certain global objectives optimally, not as an ensemble of already existing parts. The approach illustrated in this paper for aircraft systems is equally applicable to other systems where every function is driven by a finite amount of fuel installed on board – automobiles, ships, power tools, military vehicles, weapon systems and environmental control suits.

Natural flow systems are optimized and function similarly. The thought that the engineering design and constraints principle (the constructal principle) generates the optimized shape and structure of natural flow systems is the constructal theory [1]. To maximize the global performance of energy systems based on a finite amount of fuel means to focus on the thermodynamic optimization of the use of fuel. Power and refrigeration systems are assemblies of streams and hardware (components). The size of the hardware is always constrained, e.g., weight, volume, cost. Each stream carries exergy (useful work content), which is the life blood of the fuel burned in order to drive all the subsystems. Exergy is destroyed or entropy is generated whenever streams interact with each other and with components [2–4]. The route to improved global performance consists of

1. optimizing every stream–component interaction so that it destroys least exergy subject to constraints,
2. fitting the optimized entities together into a new design of the larger system.

What emerges is an exergy-based design and a visible geometry (configuration) that reflects the thermodynamic optimization principle and the various

* Corresponding author. Tel.: +1-919-660-5309; fax: +1-919-660-8963.

E-mail address: dalford@duke.edu (A. Bejan).

0017-9310/01/$ - see front matter
PII: S0017-9310(01)00033-3

Nomenclature

A	heat transfer area (m^2)
A_{cd}	diffuser inlet cross-sectional area (m^2); $\tilde{A}_{cd} = A_{cd}/(1\ m^2)$
$B_{a,e}$	channel spacings (m)
b	constant, R/c_p
c_p	specific heat at constant pressure (J/kg K)
$C_{1,2}$	factors
D_h	hydraulic diameter (m)
DHN	diffuser–heat exchanger–nozzle assembly
ECS	environmental control system
f	friction factor
F	drag force (N)
F, $\tilde{F}$	functions, Eqs. (15) and (17)
g	gravitational acceleration (m^2/s)
h	heat transfer coefficient (W/m^2 k)
H	height (m)
k	thermal conductivity (W/m K)
$K_{c,e}$	loss coefficients for contraction and enlargement
$L_{x,y,z}$	lengths (m)
$\dot{m}$	mass flow rate (kg/s)
M	mass (kg)
M	Mach number, Eq. (37)
n	number of channels
N	number of heat transfer units, Eq. (27)
N_S	entropy generation number, Eq. (18)
P	pressure (Pa)
$\tilde{P}$	dimensionless pressure, Eq. (20)
Pr	Prandtl number
R	ideal gas constant (J/kg K)
Re	Reynolds number
$\dot{S}_{gen}$	entropy generation rate (W/K)
t	thickness (m)
T	temperature (K)
U	overall heat transfer coefficient (W/m^2 K)
v	specific volume (m^3/kg)
V	velocity (m/s)
$\tilde{V}$	dimensionless velocity, Eq. (36)
V_t	total volume (m^3)
w	dimensionless power, Eq. (17)
$\dot{W}$	power (W)
x	volume scale

Greek symbols

γ	ratio of specific heats, c_p/c_v
ΔP	pressure drop (Pa)
η	isentropic efficiency
η_0	fin efficiency, Eq. (44)
μ	ratio of capacity rates, Eq. (21)
ρ	density (kg/m^3)
σ	contraction ratio
ϕ	volume fraction, Eq. (52)

Subscripts

a	ambient
b	body
c	compressor
d	diffuser
e	engine-air stream
min	minimum
n	nozzle
opt	optimum
out	outlet
rev	reversible
t	turbine
w	wall

constraints. The optima and structural characteristics identified based on thermodynamic optimization can be made more realistic through subsequent refinements based on global cost minimization, or thermoeconomics [5].

On an aircraft there are many systems and processes that contribute to the ultimate destruction of all the exergies furnished by the fuel. Fig. 1 presents a summary of the distribution of losses, highlighting the losses that will be minimized as an ensemble in this study. Proceeding in the direction of fuel flow, the first exergy loss (about 30% [6]) is due to the combustion process. Next is the loss due to the irreversible operation of the engine. The remaining exergy fraction is the power produced by the engine, which drives all the subsystems and meets all the functions of the aircraft. Chief among functions is the power required to maintain the flight ($\dot{W}$), i.e., to overcome drag and to hold (support) the aircraft at its altitude. The power $\dot{W}$ is destroyed completely in the turbulent flow around the aircraft, especially in the wake.

The rest of the power generated by the engine is destroyed in the auxiliary systems, which are numerous. The dominant user of exergy is the environmental control system (ECS), which on a military transport plane such as the C-17 accounts for 64.6% of the engine power at cruise condition [7]. The ECS itself is an assembly of subsystems, as shown in the example of Fig. 2. In the "bootstrap air cycle" a fraction of the compressed airstream is bled from the engine compressor and compressed further in a compressor driven by its own turbine. In between, the compressed "engine air" is cooled in a cross-flow heat exchanger by a stream of "ram air". The engine-air stream expanded through the turbine becomes the room temperature air needed to ventilate and cool the cabin and avionics. On the ram-

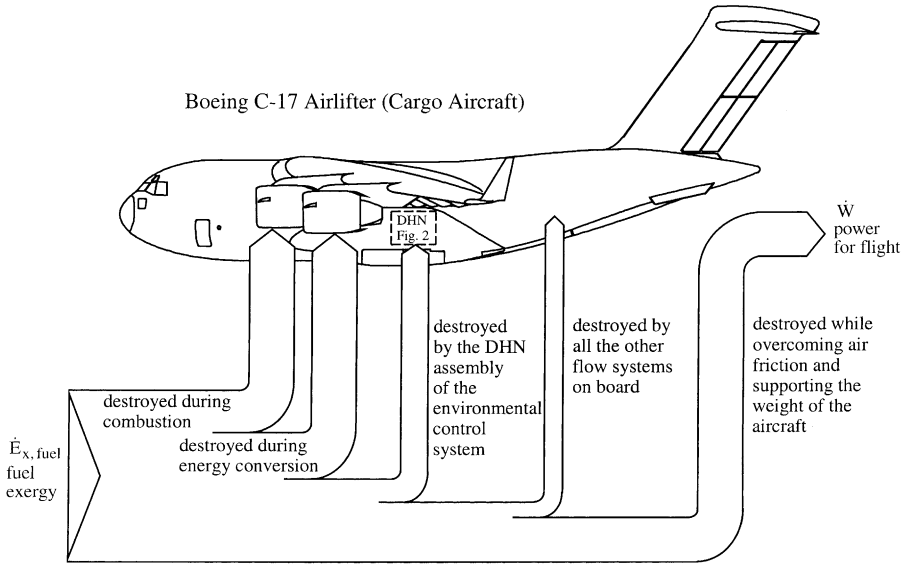

Fig. 1. The distribution of exergy destruction on an aircraft.

air side, the heat exchanger core (H) is fitted with a diffuser (D) and a nozzle (N) to decelerate and reaccelerate the ram air that initially enters the ECS at cruising speed.

We will show that the exergy destruction rate of the ECS is a strong function of the physical size of the cross-flow heat exchanger assembly – diffuser, heat exchanger, nozzle (DHN). The mass of the ECS is essentially the mass of the DHN assembly. Contemplating changes in ECS size (mass) means varying the total mass of the aircraft (M). Along with the cruising speed V, the aircraft mass is the dominant parameter that determines the exergy requirement for powered flight ($\dot{W}$). In sum, the integrative design of the ECS architecture sends us in the direction of minimizing *together* the exergy destroyed in the ECS and the exergy destroyed in powered flight. In this study we show how the structure of the DHN assembly can be derived from minimizing together the exergy losses associated with powered flight and the DHN assembly. This represents a new step beyond what is currently done in thermodynamic optimization, where heat exchangers have often been optimized individually, in isolation [3].

2. The destruction of exergy in powered flight

The relationship between flying power requirement and aircraft mass and speed can be demonstrated by analyzing the simple system shown in Fig. 3 [1]. The flying body of mass M has the linear dimension D and average density ρ_b. This leads to the global requirement that the net vertical body force $Mg \sim \rho_b D^3 g$ must be supported by other forces. The generation of such forces is achieved through flight. More elaborate models of flying bodies can be and have been used, as shown in the literature reviewed in [1].

Consider the conservation of mass and momentum in the control volume occupied by the flying body and the immediately close fluid regions affected by relative motion. In the steady state, an air stream of mass flow rate $\dot{m} \sim \rho_a D^2 V$ enters the control volume, and the same stream exits ($\dot{m} \sim \rho_a D_{out}^2 V_{out}$). The exit velocity V_{out} must have a vertical component (V_{down}) in order to develop a vertical flow of momentum to support the body force,

$$V_{out} = \left(V_x^2 + V_{down}^2\right)^{1/2}. \tag{1}$$

The vertical momentum balance is $\rho_b D^3 g \sim \dot{m} V_{down}$ or

$$V_{down} \sim \frac{\rho_b g D}{\rho_a V}. \tag{2}$$

The conservation of horizontal momentum is the statement that the momentum generated by the outflow ($\dot{m}V_x$) must balance the retarding forces associated with momentum inflow ($\dot{m}V$) and drag (F),

$$\dot{m}V_x \sim \dot{m}V + F. \tag{3}$$

The drag force F is of order $C_D D^2 \rho_a V^2$, where D^2 is the scale of the body cross-section. The drag coefficient C_D is a relatively constant number of order 1 when the Reynolds number ($\rho_a VD/\mu_a$) is greater than the order 10^2. This means that the ratio $F/\dot{m}$ scales as

$$\frac{F}{\dot{m}} \sim V. \tag{4}$$

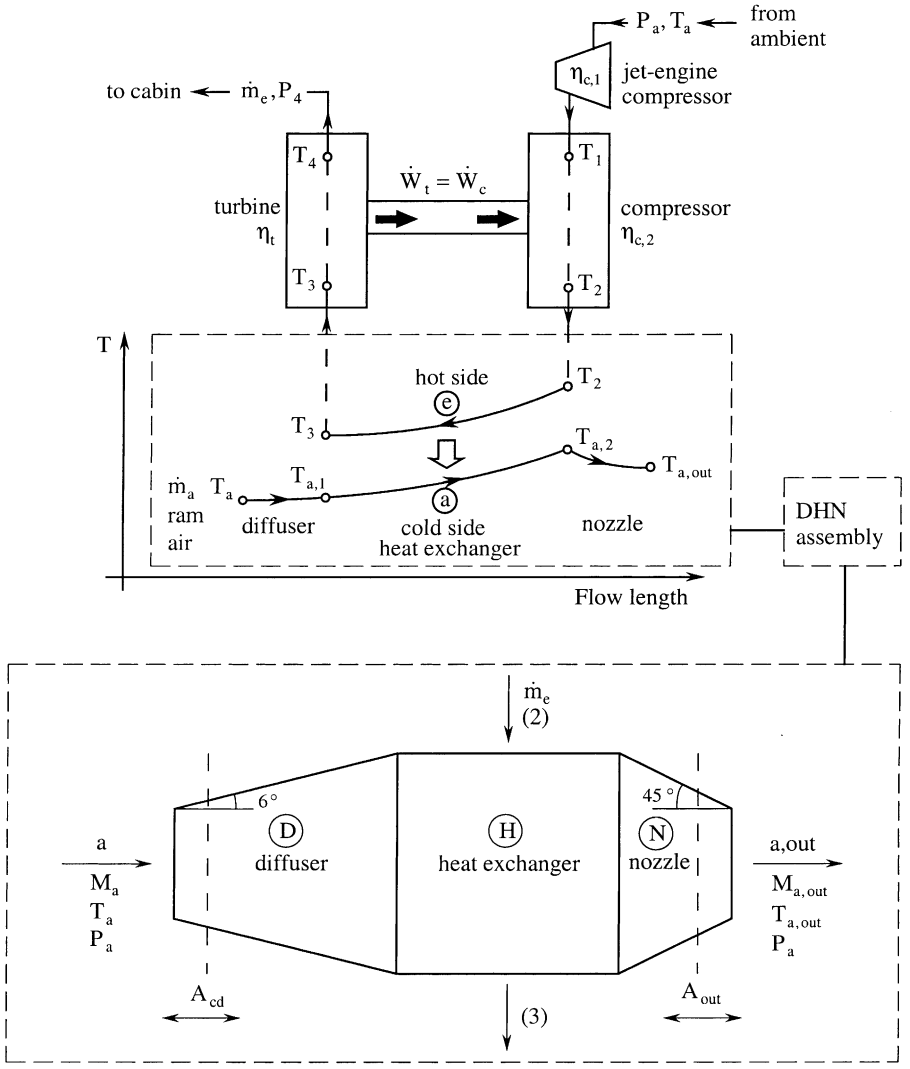

Fig. 2. ECS based on the bootstrap air cycle, and the assembly composed of the diffuser, heat exchanger and nozzle (DHN).

Finally, the flying system must spend mechanical power ($\dot{W}$) in order to increase the kinetic energy of the air stream, from the inlet ($\dot{m}V^2/2$) to the outlet ($\dot{m}V_{\text{out}}^2/2$),

$$\dot{W} \sim \frac{1}{2}\dot{m}\left(V_{\text{out}}^2 - V^2\right). \tag{5}$$

Using Eqs. (1)–(3), approximating $V_x^2 \sim (V + F/\dot{m})^2 \sim V^2 + 2VF/\dot{m}$, and neglecting all the factors of order 1, we can eliminate V_{down} and rewrite Eq. (5) as [1]

$$\dot{W} \sim \frac{\rho_b^2 g^2 D^4}{\rho_a V} + \rho_a D^2 V^3. \tag{6}$$

This two-term expression shows the power that is required to maintain the body in the air (the first term), and to overcome the drag (the second term). This function has a minimum with respect to V,

$$V_{\text{opt}} \sim \left(\frac{\rho_b}{\rho_a} gD\right)^{1/2}, \tag{7}$$

$$\dot{W}_{\min} \sim \frac{\rho_b^{3/2} g^{3/2} D^{7/2}}{\rho_a^{1/2}}. \tag{8}$$

At this optimal speed the power spent on lifting the body is three times larger than the power needed to overcome the drag. Here we have an example of optimal allocation, or optimal partition, which is a common occurrence in thermodynamic optimization [1,8]. When the flying speed is significantly less than the optimal, the

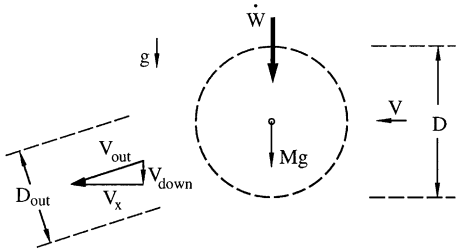

Fig. 3. Simple model and interactions of a flying body [1].

power requirement is dominated by the need to hold the body in the air. In the opposite extreme the power is spent mainly on overcoming drag. In this study we consider the general case where $V \neq V_{opt}$, and the flying power requirement is given by the two-term expression (6).

3. Exergy destruction in powered flight and ECS

The exergy destruction rate associated with every compartment of the aircraft is proportional to the rate of entropy generation in that compartment. This proportionality is known as the Guoy-Stodola theorem [2,3]. The exergy destruction rate in the heat exchanger of the ECS is $T_a\dot{S}_{gen,DHN}$, where T_a is the temperature of the ambient. The establishment of $\dot{S}_{gen,DHN}$ as a function of the geometric and flow parameters of the heat exchanger is the subject of the thermo-fluid analysis outlined in the next section. Here we express analytically the message of Fig. 1, which is that the exergy flow rate brought in by the fuel is destroyed by flying ($\dot{W}$), the ECS ($T_a\dot{S}_{gen,DHN}$) and the rest of the components and processes ($T_a\dot{S}_{gen,rest}$). The latter include the combustion, the irreversibility of the engine and the power used by the remaining systems of the aircraft,

$$\dot{E}_{x,fuel} = \dot{W} + T_a\dot{S}_{gen,DHN} + T_a\dot{S}_{gen,rest}. \quad (9)$$

Changes in the configuration and size of the heat exchanger affect only the first two terms on the right-hand side of Eq. (9). The $\dot{W}$ term is itself the sum of two terms that depend on the mass of the aircraft cf. Eq. (6). Instead of using the mass, we rewrite $\dot{W}$ in terms of the volume scale,

$$x = M/\rho_b. \quad (10)$$

In Eq. (10) the density of the flying body ρ_b is the average density of all the components and materials that make up the airplane. The average density is computed based on the linear dimension of the space occupied by the airplane (D) and the total mass of the airplane (M), cf. Table 1,

$$\rho_b \sim M/D^3. \quad (11)$$

Table 1
Physical values used as reference case in the numerical optimization of the overall system

$c_p = 1$ kJ kg^{-1} K^{-1}	$T_a = 244.5$ K
$D = 35$ m	$T_4 = 283.2$ K
$k_w = 20.8$ W m^{-1} K^{-1}	$V_t = 1$ m^3
$\dot{m}_e = 0.7$ kg s^{-1}	$\gamma = 1.4$
$M = 10^5$ kg	$\eta_{c,1} = 0.9$
$P_a = 0.03$ MPa	$\eta_{c,2} = 0.7$
$P_4 = 0.1$ MPa	$\eta_d = 0.97$
$Pr = 0.72$	$\eta_n = 0.95$
$R = 287$ J kg^{-1} K^{-1}	$\eta_t = 0.8$
$t_w = 0.6$ mm	

We distinguish between volumes of the diffuser, heat exchanger and nozzle (x_{DHN}) and the rest of the aircraft and ECS (x_{rest}),

$$x = x_{DHN} + x_{rest}. \quad (12)$$

The x_{rest} volume is several orders of magnitude larger than x_{DHN}, and is constant; x_{rest} also includes the volume of the compressor, turbine and ducting of the remainder of the ECS, Fig. 2.

The function $\dot{W}(x)$ is provided by Eq. (6) in combination with $M \sim \rho_b D^3$ and Eq. (10),

$$\dot{W} \sim C_1 x^{4/3} + C_2 x^{2/3}, \quad (13)$$

where $C_1 = \rho_b^2 g^2/(\rho_a V)$ and $C_2 = \rho_a V^3$. Linearizing this expression in the vicinity of $x = x_{rest}$, where $(x - x_{rest}) \ll x_{rest}$, we use

$$\dot{W} \cong \dot{W}(x_{rest}) + \left(\frac{d\dot{W}}{dx}\right)_{x_{rest}} (x - x_{rest}), \quad (14)$$

where

$$x - x_{rest} = x_{DHN},$$

and

$$\left(\frac{d\dot{W}}{dx}\right)_{x_{rest}} = \frac{4}{3}C_1 x_{rest}^{1/3} + \frac{2}{3}C_2 x_{rest}^{-1/3}.$$

The second term on the right-hand side of Eq. (9) varies as $\dot{S}_{gen,DHN}(x_{DHN})$, while $\dot{S}_{gen,rest}$ is independent of x_{DHN}.

In summary, Eq. (9) can be rearranged to show the overall quantity (F) that varies with the volume of the DHN assembly:

$$F = \dot{E}_{x,fuel} - \dot{W}(x_{rest}) - T_a\dot{S}_{gen,rest} = \left(\frac{d\dot{W}}{dx}\right)_{x_{rest}} x_{DHN} + T_a\dot{S}_{gen,DHN}. \quad (15)$$

Nondimensionalizing this expression with respect to $\dot{m}_e c_{pe} T_4$, where $\dot{m}_e$ and T_4 are defined in Fig. 2, we obtain

$$\tilde{F} = w + \tau_a N_S, \tag{16}$$

$$\tilde{F} = F/(\dot{m}_e c_{pe} T_4), \quad w = \left(\frac{d\dot{W}}{dx}\right)_{x_{rest}} \frac{x_{DHN}}{\dot{m}_e c_{pe} T_4}, \tag{17}$$

$$\tau_a = T_a/T_4, \quad N_S = \dot{S}_{gen,DHN}/(\dot{m}_e c_{pe}). \tag{18}$$

The objective of the following study is to minimize $\tilde{F}$ by properly selecting the structure and size of the DHN assembly and its components. The first term of the $\tilde{F}$ expression accounts for the effect of x_{DHN} on the flying power requirement of the aircraft. The second term accounts for the exergy destroyed by the ECS, as shown by the analysis presented in the next section.

4. ECS model

Consider the model with two streams shown in Fig. 2 (top). The upper stream $\dot{m}_e$ is originally drawn from the ambient (P_a, T_a), and is compressed to the state (P_1, T_1) in the low-pressure stages of the jet engine. This "engine" air stream $(\dot{m}_e)$ is a fraction of the air flow rate processed by the jet-engine compressor. The stream $\dot{m}_e$ is compressed further in a separate compressor, which raises its pressure and temperature (P_2, T_2). Next, the stream temperature is lowered to T_3 in a cross-flow heat exchanger, and then the stream is expanded through a turbine. The shaft power produced by the turbine is used to drive the separate compressor, $\dot{W}_t = \dot{W}_c$. The purpose of the expansion through the turbine is to decrease the pressure and temperature to the specified cabin conditions (P_4, T_4). The air flow rate $\dot{m}_e$ is also specified by the environmental design of the cabin.

The lower stream $\dot{m}_a$ shown in Fig. 2 (top) is the ram air used on the cold side of the cross-flow heat exchanger. The ram air enters the system at ambient conditions (P_a, T_a), and initially it has the same speed as the aircraft (V_a). It is decelerated to the state (a,1) in a diffuser, and continues through the heat exchanger, where it is heated to the state (a,2). Before being discharged into the ambient, the $\dot{m}_a$ stream is accelerated to the state (a,out). The ram-air mass flow rate $\dot{m}_a$ is not specified.

Fig. 2 (bottom) shows the DHN assembly. The physical size of the DHN assembly varies in the optimization process, according to the variation of the diffuser inlet area, nozzle outlet area and heat exchanger geometry. The truncated cone half-angles of the diffuser (6°) and nozzle (45°) are also indicated in Fig. 2: these values were taken as standards used in the aircraft industry [9].

The processes undergone by the engine-air and ram-air streams are shown in their respective T–s diagrams in Fig. 4. Every process is irreversible. Fig. 4(a) shows that the compression process (1)–(2) is not isentropic: the isentropic efficiency is $\eta_{c,2} < 1$. Similarly, the expansion (3)–(4) is characterized by the turbine isentropic efficiency $\eta_t < 1$. The flow (2)–(3) on the hot side of the heat exchanger is accompanied by the frictional pressure drop ΔP_e. The preliminary compression (a)–(1) executed in the jet-engine compressor is not shown; its isentropic efficiency is $\eta_{c,1} < 1$.

Fig. 4(b) shows the deceleration process (a)–(a,1) through the diffuser, where the isentropic efficiency is η_d. The pressure drop experienced by the ram air while flowing on the cold side of the heat-exchanger surface is ΔP_a. The isentropic efficiency of the nozzle acceleration process (a,2)–(a,out) is η_n.

5. Entropy generation analysis

The analysis developed in this section establishes the relation between the entropy generation rate and the physical features of the system. To start with, the entropy generation rate due to the complete system defined in Fig. 2 is

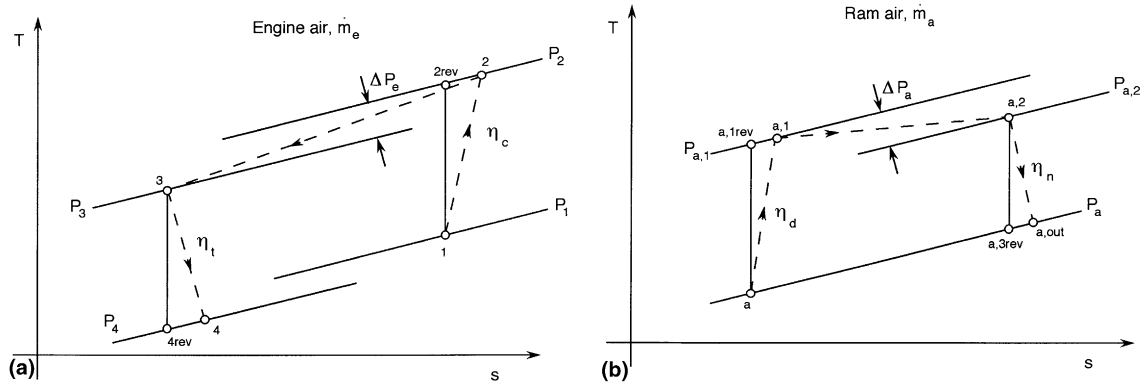

Fig. 4. The T–s diagrams for the processes undergone by the engine-air and ram-air streams of the ECS heat exchanger.

$$\dot{S}_{\mathrm{gen,DHN}} = \dot{m}_{\mathrm{e}}\left[\left(c_{\mathrm{p}}\ln\frac{T_1}{T_{\mathrm{a}}} - R\ln\frac{P_1}{P_{\mathrm{a}}}\right) + \left(c_{\mathrm{p}}\ln\frac{T_2}{T_1} - R\ln\frac{P_2}{P_1}\right) + \left(c_{\mathrm{p}}\ln\frac{T_3}{T_2} - R\ln\frac{P_3}{P_2}\right) + \left(c_{\mathrm{p}}\ln\frac{T_4}{T_3} - R\ln\frac{P_4}{P_3}\right)\right]_{\mathrm{e}} + \dot{m}_{\mathrm{a}}\left(c_{\mathrm{p}}\ln\frac{T_{\mathrm{out}}}{T_{\mathrm{in}}} - R\ln\frac{P_{\mathrm{out}}}{P_{\mathrm{in}}}\right)_{\mathrm{a}}. \quad (19)$$

The terms collected in this expression correspond to the sequence of components recognized in Figs. 2 and 4. The two fluids are modeled as ideal gases with constant specific heat, $(R, c_{\mathrm{p}})_{\mathrm{e}}$ and $(R, c_{\mathrm{p}})_{\mathrm{a}}$. It is convenient to introduce the nondimensional variables

$$\tilde{P} = \frac{P}{P_4}, \quad \tau = \frac{T}{T_4}, \quad (20)$$

$$\mu = \frac{\dot{m}_{\mathrm{a}}c_{\mathrm{pa}}}{\dot{m}_{\mathrm{e}}c_{\mathrm{pe}}}, \quad (21)$$

where P_4, T_4, and $\dot{m}_{\mathrm{e}}$ are the fixed cabin conditions, N_{S} is the entropy generation number, and μ is the ratio of the two capacity rates. Eq. (19) becomes

$$N_{\mathrm{S}} = \left(\ln\frac{\tau_1}{\tau_{\mathrm{a}}} - b\ln\frac{\tilde{P}_1}{\tilde{P}_{\mathrm{a}}}\right) + \left(\ln\frac{\tau_2}{\tau_1} - b\ln\frac{\tilde{P}_2}{\tilde{P}_1}\right) + \left(\ln\frac{\tau_3}{\tau_2} - b\ln\frac{\tilde{P}_3}{\tilde{P}_2}\right) + \left(\ln\frac{1}{\tau_3} - b\ln\frac{1}{\tilde{P}_3}\right) + \mu\ln\frac{\tau_{\mathrm{a,out}}}{\tau_{\mathrm{a}}}, \quad (22)$$

where $b = R/c_{\mathrm{p}}$. It is assumed that the two streams have the same b value, namely $b = 0.286$, which corresponds to $\gamma = c_{\mathrm{p}}/c_{\mathrm{v}} = 1.4$. Eq. (22) was abbreviated based on the observation that $P_{\mathrm{out}} = P_{\mathrm{in}} = P_{\mathrm{a}}$.

In the method of entropy generation minimization [3] the entropy generation calculation is complemented by the analysis of the heat flow and fluid flow through each component. This analysis accounts for the physical parameters and size constraints of the component. For the first component of our system – the engine compressor (a)–(1) in Fig. 2 – these effects are embodied in the specified compressor efficiency

$$\eta_{\mathrm{c,1}} = \frac{T_{1,\mathrm{rev}} - T_{\mathrm{a}}}{T_1 - T_{\mathrm{a}}}. \quad (23)$$

Noting that $T_{1,\mathrm{rev}} = T_{\mathrm{a}}(P_1/P_{\mathrm{a}})^b$, Eq. (23) becomes

$$\tau_1 = \tau_{\mathrm{a}} + \frac{\tau_{\mathrm{a}}}{\eta_{\mathrm{c,1}}}\left[\left(\frac{\tilde{P}_1}{\tilde{P}_{\mathrm{a}}}\right)^b - 1\right]. \quad (24)$$

Next, for the separate compressor (1) and (2) the definition of the isentropy efficiency $\eta_{\mathrm{c,2}}$ and the first-law analysis yield

$$\tau_2 = \tau_1 + \frac{\tau_1}{\eta_{c,2}}\left[\left(\frac{\tilde{P}_2}{\tilde{P}_1}\right)^b - 1\right], \quad (25)$$

$$w_{\mathrm{c}} = \frac{\tau_1}{\eta_{\mathrm{c,2}}}\left[\left(\frac{\tilde{P}_2}{\tilde{P}_1}\right)^b - 1\right]. \quad (26)$$

In Eq. (26) the compressor power input w_{c} is dimensionless,

$$w_{\mathrm{c}} = \dot{W}_{\mathrm{c}}/(\dot{m}_{\mathrm{e}}c_{\mathrm{pe}}T_4).$$

The heat transfer between the two streams in the cross-flow heat exchanger is described by the effectiveness-NTU relation [10]

$$\varepsilon = 1 - \exp\left\{\mu N^{0.22}\left[\exp\left(-\mu^{-1}N^{0.78}\right) - 1\right]\right\}, \quad (27)$$

which is based on the assumption that $\dot{m}_{\mathrm{e}}c_{\mathrm{pe}}$ is the smaller of the two capacity rates (i.e., $\mu > 1$), and where N is the number of heat transfer units, $N = UA/(\dot{m}_{\mathrm{e}}c_{\mathrm{pe}})$. The definition of the effectiveness ε produces two reactions between the inlet and outlet temperatures of the two streams,

$$\tau_2 - \tau_3 = \varepsilon(\tau_2 - \tau_{\mathrm{a,1}}), \quad (28)$$

$$\tau_{\mathrm{a,2}} - \tau_{\mathrm{a,1}} = \frac{\varepsilon}{\mu}(\tau_2 - \tau_{\mathrm{a,1}}). \quad (29)$$

Eqs. (27)–(29) hold for $\mu > 1$; the corresponding set for $\mu < 1$ is not listed, for the sake of brevity. The pressure drop along the hot side of the heat transfer surface, $\Delta\tilde{P}_{\mathrm{e}} = \tilde{P}_2 - \tilde{P}_3$, is analyzed later in this section.

Downstream of the cross-flow heat exchanger is the turbine (3)–(4): the definition of the efficiency η_t, and the first-law analysis of the turbine yield

$$\tau_3 = 1 + \eta_{\mathrm{t}}\tau_3\left(1 - \tilde{P}_3^{-b}\right), \quad (30)$$

$$w_{\mathrm{t}} = \eta_{\mathrm{t}}\tau_3\left(1 - \tilde{P}_3^{-b}\right). \quad (31)$$

The dimensionless turbine power output is defined as $w_{\mathrm{t}} = \dot{W}_{\mathrm{t}}/(\dot{m}_{\mathrm{e}}c_{\mathrm{pe}}T_4)$. Finally, since the turbine drives the separate compressor, $w_{\mathrm{t}} = w_{\mathrm{c}}$ (a special case in fact), the first-law analysis of the turbine and compressor (together) requires

$$\tau_2 - \tau_1 = \tau_3 - 1. \quad (32)$$

On the cold side of the system, we analyze the course followed by the ram air. This begins with the diffuser (a)–(a,1), for which the η_{d} definition and the first law of thermodynamics require

$$\eta_{\mathrm{d}} = \frac{T_{\mathrm{a,1rev}} - T_{\mathrm{a}}}{T_{\mathrm{a,1}} - T_{\mathrm{a}}}, \quad (33)$$

$$c_{pa}(T_{a,1}-T_a)=\frac{1}{2}\left(V_a^2-V_{a,1}^2\right), \tag{34}$$

where $T_{a,1rev}=T_a(P_{a,1}/P_a)^b$. The dimensionless version of Eqs. (33) and (34) is

$$\frac{\tau_{a,1}}{\tau_a}-1=\frac{1}{\eta_d}\left[\left(\frac{\tilde{P}_{a,1}}{\tilde{P}_a}\right)^b-1\right], \tag{35}$$

$$\frac{\tau_{a,1}}{\tau_a}-1=\frac{1}{2}\left(\tilde{V}_a^2-\tilde{V}_{a,1}^2\right). \tag{36}$$

The dimensionless bulk velocity $\tilde{V}=V/(c_{pa}T_a)^{1/2}$ is proportional to the Mach number $M=V/(\gamma_a R_a T_a)^{1/2}$, or $\tilde{V}=M(\gamma_a-1)^{1/2}$. Invoking the conservation of the mass flow rate $\dot{m}_a$ in every cross-section A_c and the ideal gas model, namely $\dot{m}_a=\rho V A_c$ and $\rho=P/(RT)$, we write the Mach number as

$$M=\frac{\dot{m}_a}{PA_c}\left(\frac{R_a}{\gamma_a}T\right)^{1/2} \tag{37}$$

In sum, when the geometry and operating conditions are specified, Eqs. (35)–(37) pinpoint state (a,1), or $\tilde{P}_{a,1}$ and $\tau_{a,1}$.

The heating process (a,1)–(a,2) experienced by the $\dot{m}_a$ stream is governed by the effectiveness–NTU relations (27)–(29). The pressure drop $\Delta\tilde{P}_a=\tilde{P}_{a,1}-\tilde{P}_{a,2}$ is given by Eq. (42) later in this section.

Finally, the irreversible flow through the nozzle is described by the efficiency and first-law relations

$$\eta_n=\frac{T_{a,2}-T_{a,out}}{T_{a,2}-T_{a,out\ rev}}, \tag{38}$$

$$c_{pa}(T_{a,2}-T_{a,out})=\frac{1}{2}\left(V_{a,out}^2-V_{a,2}^2\right). \tag{39}$$

Recognizing $T_{a,out\ rev}=T_{a,2}(P_a/P_{a,2})^b$ and the nondimensional variables employed earlier, we can nondimensionalize Eqs. (38) and (39) as

$$1-\frac{\tau_{a,out}}{\tau_{a,2}}=\eta_n\left[1-\left(\frac{\tilde{P}_a}{\tilde{P}_{a,2}}\right)^b\right], \tag{40}$$

$$\frac{\tau_{a,2}}{\tau_a}-\frac{\tau_{a,out}}{\tau_a}=\frac{1}{2}\left(\tilde{V}_{a,out}^2-\tilde{V}_{a,2}^2\right). \tag{41}$$

For the pressure drops along the counterflow $(\Delta P_e, \Delta P_a)$ we use the classical formulation [11]

$$\Delta P_i=\frac{1}{2}G_i^2 v_{i,in}\left[\left(K_{c,i}+1-\sigma_i^2\right)+2\left(\frac{v_{i,out}}{v_{i,in}}-1\right)+f_i\frac{A_i}{A_{c,i}}\frac{\overline{v_i}}{v_{i,in}}-\left(1-\sigma_i^2-K_{e,i}\right)\frac{v_{i,out}}{v_{i,in}}\right],\quad (i=e,a), \tag{42}$$

where

$$\overline{v_i}=\frac{1}{2}(v_{i,in}+v_{i,out}),\quad \sigma_{in}=\frac{A_{c,i}}{A_{f,i}}. \tag{43}$$

In these relations G_i, v_i, A_i, f_i, σ_i, $K_{c,i}$, $K_{e,i}$, $A_{c,i}$ and $A_{f,i}$ represent in order, the mass velocity ($G_i=\dot{m}_i/A_{c,i}$), the specific volume ($v_i=R_iT_i/P_i$), the total heat transfer area, the friction factor, the cross-sectional contraction ratio, the contraction loss coefficient, the enlargement loss coefficient, the flow cross-section and the stream cross-section before entering the duct. The friction factor is available as a function of the Reynolds number based on hydraulic diameter, $f_i=f_i(Re_i)$, either as empirical correlations for parallel-plate channels, or as tabulated data for finned surfaces [11].

The same heat exchanger sources provide the heat transfer coefficient information needed for evaluating the number of heat transfer units N. The flow of heat across the A_i surface overcomes three thermal resistances in series,

$$\frac{1}{N}=\frac{\dot{m}_e c_{pe}}{UA}=\dot{m}_e c_{pe}\left(\frac{1}{\eta_{0,e}h_e A_e}+\frac{t_w}{k_w A_w}+\frac{1}{\eta_{0,a}h_a A_a}\right). \tag{44}$$

In this expression $\eta_{0,i}$, t_w, k_w and A_w are the fin efficiencies of the finned surfaces, the thickness of the wall penetrated by heat transfer, the wall thermal conductivity, and the average heat transfer surface, $A_w=(A_e+A_a)/2$. The heat transfer coefficients (h_e, h_a) are available in dimensionless form, as the respective Stanton number versus the channel Reynolds number, $h_i/(c_{pi}G_i)=St_i(Re_i)$.

5.1. Parallel-plate heat exchanger

The preceding analysis completes the model, and allows us to relate N_S to the irreversibilities and physical sizes of all the components. The numerical minimization of the entropy generation rate can proceed, but first we must specify the type of the heat transfer surface built into the cross-flow heat exchanger. This assumption is necessary in order to access the f_i and St_i information that is available in the heat exchanger literature.

In this optimization study we assumed the simplest and best documented surface type: parallel plates of spacings B_e and B_a, as shown in Fig. 5. For the laminar regime ($Re_{D_h}<2300$) we used the friction factor and heat transfer coefficient correlations (e.g., [12]),

$$f_i=\frac{24}{Re_{D_{h,i}}},\quad \frac{h_i D_{h,i}}{k_i}=8.235, \tag{45}$$

where $D_{h,i}=2B_i$, $Re_{D_{h,i}}=G_iD_{h,i}/\mu_i$ and $i=e,a$. The correlations used for the turbulent regime were [12]

$$f_i=0.079Re_{D_{h,i}}^{-1/4}\quad \left(2300<Re_{D_{h,i}}<2\times10^4\right), \tag{46}$$

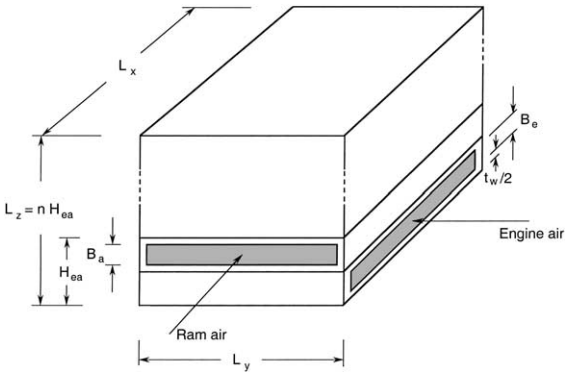

Fig. 5. The geometric features of the core of a parallel-plate cross-flow heat exchanger.

$$\frac{h_i D_{\mathrm{h},i}}{k_i} = \frac{(f_i/2)\left(Re_{D_{\mathrm{h},i}} - 10^3\right)Pr_i}{1 + 12.7(f_i/2)^{1/2}\left(Pr_i^{2/3} - 1\right)} \quad \left(2300 < Re_{D_{\mathrm{h},i}} < 5 \times 10^6\right). \tag{47}$$

The height H_{ea} of the elemental channel unit is defined as the height of the assembly composed of one engine-air passage and one ram-air passage,

$$H_{\mathrm{ea}} = B_{\mathrm{e}} + B_{\mathrm{a}} + 2t_{\mathrm{w}}. \tag{48}$$

If n is the number of elemental units in the stack, the height of the heat exchanger core is

$$L_z = nH_{\mathrm{ea}}. \tag{49}$$

The total volume of the core is constrained, $V_{\mathrm{t}} = L_x L_y L_z$, constant or, nondimensionally, as $\tilde{V}_{\mathrm{t}} = V_{\mathrm{t}}/(1\ \mathrm{m}^3)$. The length scale $V_{\mathrm{t}}^{1/3}$ is used for the purpose of nondimensionalizing all the lengths that characterize this geometry,

$$(\tilde{B}_{\mathrm{e}}, \tilde{B}_{\mathrm{a}}, \tilde{t}_{\mathrm{w}}, \tilde{H}_{\mathrm{ea}}, \tilde{L}_x, \tilde{L}_y, \tilde{L}_z) = (B_{\mathrm{e}}, B_{\mathrm{a}}, t_{\mathrm{w}}, H_{\mathrm{ea}}, L_x, L_y, L_z)/V_{\mathrm{t}}^{1/3} \tag{50}$$

such that the volume constraint reads

$$\tilde{L}_x \tilde{L}_y \tilde{L}_z = 1. \tag{51}$$

Another constraint that we attach to the geometric optimization procedure is the total volume (or weight) of the wall material, $2nL_xL_yt_{\mathrm{w}}$. This second constraint is best represented by the volume fraction ϕ ($\ll 1$) occupied by the wall material in the entire volume, $\phi = 2nL_xL_yt_{\mathrm{w}}/V_{\mathrm{t}}$, constant, or

$$\phi = 2n\frac{\tilde{t}_{\mathrm{w}}}{\tilde{L}_z} = 2n\tilde{L}_x\tilde{L}_y\tilde{t}_{\mathrm{w}} \quad \text{(constant)}. \tag{52}$$

The diffuser is characterized by its inlet cross-sectional area, A_{cd}, or, nondimensionally, $\tilde{A}_{\mathrm{cd}} = A_{\mathrm{cd}}/(1\ \mathrm{m}^2)$, which is taken as an additional external parameter in the design.

According to Fig. 5, the architecture of the heat exchanger core is determined completely if we specify six dimensions: L_x, L_y, L_z, B_{e}, B_{a} and t_{w}. There are two constraints, Eqs. (51) and (52), and the reasonable assumption that the wall thickness is a specified parameter ($\tilde{t}_{\mathrm{w}} \ll 1$) dictated by the availability of standard sizes of sheet metal. In conclusion, the geometric design of the core has 3 degrees of freedom.

5.2. Optimized structure

The ECS model allows the computation of the global (aircraft level) impact associated with changes in the ECS geometry: this is represented by the function F, which is defined by Eqs. (15) and (16). This is possible once physical values (Table 1), a set of external parameters (M, $\tilde{A}_{\mathrm{cd}}$, ϕ, $\tilde{V}_{\mathrm{t}}$ and $\tilde{P}_{\mathrm{l}}$) and the set of geometric parameters (L_y/L_x, L_z/L_x and $B_{\mathrm{e}}/B_{\mathrm{a}}$) are chosen for the overall system. Eqs. (23)–(52) are then combined to form a nonlinear system of 11 nondimensional equations and 11 unknowns ($\tau_{\mathrm{a},1}$, $\tilde{P}_{\mathrm{a},1}$, $\tau_{\mathrm{a},2}$, $\tilde{P}_{\mathrm{a},2}$, τ_2, $\tilde{P}_2$, τ_3, $\tilde{P}_3$, ε, $\tilde{A}_{\mathrm{c,out}}$ and $\tau_{\mathrm{a,out}}$). This system was solved by functional iteration. A maximum tolerance of 10^{-6} was imposed on $\|R\|$, which is the residual norm of the resulting system of nonlinear equations. The numerical optimization was performed by varying the set of geometric parameters (L_y/L_x, L_z/L_x and $B_{\mathrm{e}}/B_{\mathrm{a}}$), for each set of external parameters (M, $\tilde{A}_{\mathrm{cd}}$, ϕ, $\tilde{V}_{\mathrm{t}}$ and $\tilde{P}_{\mathrm{l}}$), and identifying the optimal set of geometric parameters such that $\tilde{F}$ was minimum.

We found numerically that $\tilde{F}$ has minima with respect to each of the 3 degrees of freedom. We performed the minimization of $\tilde{F}$ in a sequence of three nested loops, first with respect to $B_{\mathrm{e}}/B_{\mathrm{a}}$, and then L_y/L_x and L_z/L_x. In this section we report only the results of the complete 3-way minimization, and how these results are affected by changes in the external parameters that remain to be specified.

Fig. 6 shows the optimal configuration for minimum exergy destruction at the global level, and the effect of

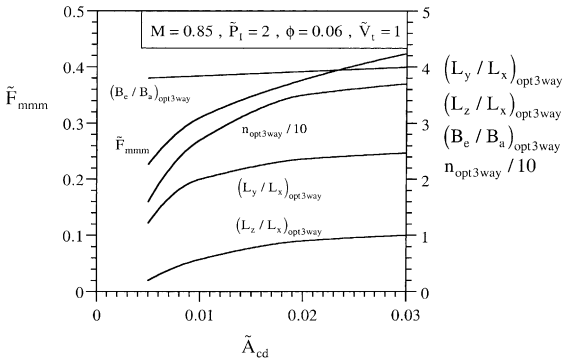

Fig. 6. The effect of the diffuser size ($\tilde{A}_{\mathrm{cd}}$) on the rate of exergy destruction at the global level ($\tilde{F}_{\mathrm{mmm}}$).

changing the diffuser cross-sectional area $\tilde{A}_{cd}$. The optimization was subjected to constant M, $\tilde{P}_l$, ϕ and $\tilde{V}_t$. The optimal configuration is represented by the aspect ratios $(B_e/B_a, L_y/L_x, L_z/L_x)_{opt3way}$. A related feature is the number of channels $n_{opt3way}$, which is also shown. The effect of the diffuser size is to increase the three aspect ratios, although this effect becomes weaker as $\tilde{A}_{cd}$ increases. The effect of $\tilde{A}_{cd}$ on $(B_e/B_a)_{opt3way}$ is weak throughout. The rate of exergy destruction ($\tilde{F}_{mmm}$, or $\tilde{F}_{opt3way}$) increases monotonically as the diffuser size increases.

Figs. 7–10 complete the reporting of how the 3-way optimized heat exchanger geometry affects the global rate of exergy destruction. Fig. 7 shows the effect of the pressure level from which the engine air is drawn, $\tilde{P}_l$. The aspect ratios $(B_e/B_a, L_z/L_x)_{opt3way}$ are practically insensitive to changes in $\tilde{P}_l$. The minimized rate of exergy destruction increases sensibly as $\tilde{P}_l$ increases.

The effect of the cruising speed (M) is documented in Fig. 8. All three geometric aspect ratios are sensitive to changes in M, however, the respective orders of magnitude of these ratios do not change relative to what we saw in Figs. 6 and 7. Expected is the increase in exergy destruction ($\tilde{F}_{mmm}$) as the cruising speed increases.

Important to documenting the effects of weight and volume on global exergy destruction are the charts of Figs. 9 and 10. The solid volume fraction (ϕ) on the abscissa of Fig. 9 is proportional to the weight of the heat exchanger, because the volume $\tilde{V}_t$ is fixed. The exergy destruction rate increases almost linearly with ϕ. The ratio of channel spacings is relatively insensitive to changes in ϕ.

Qualitatively similar trends emerge when the total volume ($\tilde{V}_t$) varies, while the solid volume fraction is held constant (ϕ), Fig. 10. A larger volume means a heavier heat exchanger and, according to the $\tilde{F}_{mmm}$ curve, a larger rate of exergy destruction.

One feature that unites the optimized geometric results reported in Figs. 6–10 is the relative insensitivity of

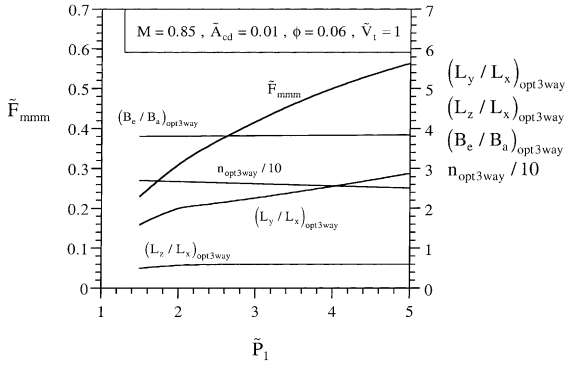

Fig. 7. The effect of the engine-air inlet pressure ($\tilde{P}_l$) on the rate of exergy destruction at the global level ($\tilde{F}_{mmm}$).

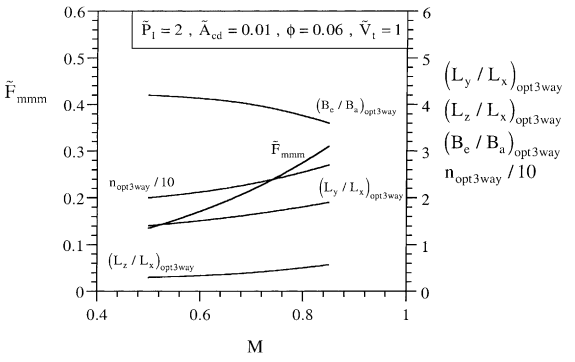

Fig. 8. The effect of the cruising speed (M) on the rate of exergy destruction at the global level ($\tilde{F}_{mmm}$).

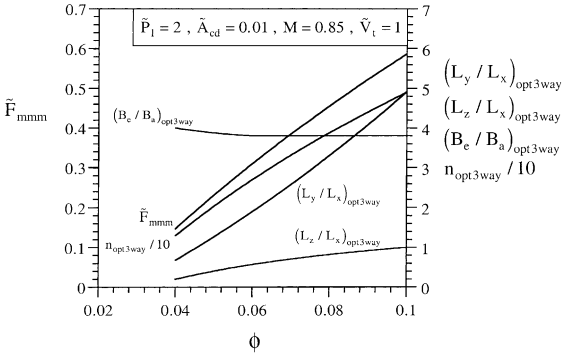

Fig. 9. The effect of the solid volume fraction (ϕ) on the rate of exergy destruction at the global level ($\tilde{F}_{mmm}$).

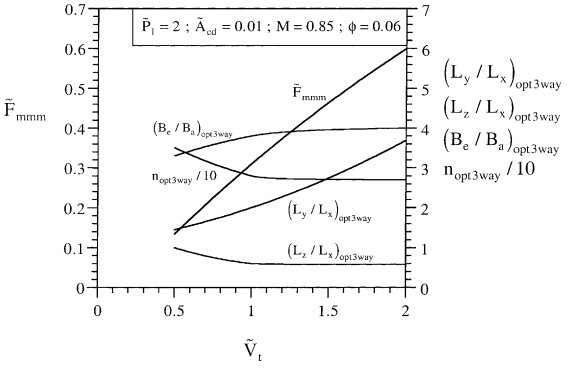

Fig. 10. The effect of the heat exchanger volume ($\tilde{V}_t$) on the rate of exergy destruction at the global level ($\tilde{F}_{mmm}$).

several aspects of the geometry when the specified external parameters change. This behavior lends "robustness" to the optimized architecture: the optimized structure performs in a nearly optimal fashion even when the prescribed or unforeseen changes in external pa-

rameters push the design away from the optimum for which the structure was actually determined. Robustness is valuable not only during operation but also in the design work itself. For example, the notion that $(B_e/B_a)_{opt3way}$ has a value approximately equal to 4 throughout the domain covered by Figs. 6–10 means that the optimal design domain can be extended more easily (approximately) by assuming $B_e/B_a \sim 4$, and minimizing $\tilde{F}$ in only two ways, with respect to L_y/L_x and L_z/L_x.

6. Concluding remarks

In this paper we illustrated an integrative approach to the thermodynamic optimization of components for energy systems. Instead of isolating (cutting away) the component from the larger system and optimizing it individually, we optimized the larger system with the component in it. We accomplished this by maximizing the global performance of the system, while varying the geometric configuration of the component.

In the example treated in this paper, the component was the cross-flow heat exchanger of the ECS of an aircraft. The larger system was the aircraft itself. The objective was to optimize the global thermodynamic performance of the aircraft, which is the same as minimizing the destruction of exergy or the consumption of fuel. We showed that the heat exchanger design impacts the global performance in two ways, through its own irreversibility, and through its contribution to the power required for sustaining the flight. The combined effect of these two contributions is expressed by the function F, Eq. (15). The minimization of F delivered the optimal structure of the heat exchanger. Every geometric feature of the heat exchanger was derived from the global optimization of performance at the aircraft level. Said another way, in our search for maximal global performance the component "morphed" into the optimal architecture summarized in charts such as Figs. 6–10.

The numerical optimization of the component geometry was conducted in dimensionless terms, in order to maximize their generality, and to minimize the number of remaining parameters that had to be specified. Regarding the latter, we found that the optimized geometry is robust relative to changes in several important operational characteristics. Robustness is a valuable feature of the design, because it simplifies the design and, once built, the system has the ability to perform at near-optional levels over a wide range of operating conditions.

Heat exchangers are virtually everywhere in engineering, even though the example treated in this paper referred to the global optimization of aircraft. The same integrative design approach is valid and deserves to be pursued in other systems where all the functions are driven by the exergy drawn from the limited fuel installed onboard e.g., ships, automobiles, military vehicles, environmental-control suits, and portable power tools.

Acknowledgements

The authors acknowledge with gratitude the guidance provided in this research project by Mr. David L. Siems of the Boeing Corporation. This material is based upon work supported by the Air Force Office of Scientific Research under Contract No. F49620-98-C-0007. Any opinions, findings and conclusions or recommendations are those of the authors and do not necessarily reflect the views of the Air Force Office of Scientific Research.

References

[1] A. Bejan, Shape and Structure, from Engineering to Nature, Cambridge University Press, Cambridge, 2000.
[2] M.J. Moran, Availability Analysis: A Guide to Efficient Energy Use, Prentice-Hall, Englewood Cliffs, NJ, 1982.
[3] A. Bejan, Advanced Engineering Thermodynamics, second ed., Wiley, New York, 1997.
[4] M. Feidt, Thermodynamique et Optimisation Energetique des Systemes et Procedes, Techique et Documentation, second ed., Lavoisier, Paris, 1996.
[5] A. Bejan, G. Tsatsaronis, M. Moran, Thermal Design and Optimization, Wiley, New York, 1996.
[6] W.R. Dunbar, N. Lior, Understanding combustion irreversibility, AES-Vol. 25/HTD-Vol. 191, Second Law Analysis-Industrial and Environmental Applications, ASME, New York, 1991, pp. 81–90.
[7] D.L. Siems, Personal communication, Boeing Corporation, 14 August 2000.
[8] A. Bejan, D. Tondeur, Equipartition, optimal allocation, and the constructal approach to predicting organization in nature, Revue Génerale de Thermique 37 (1998) 165–180.
[9] R.R. Dieckmann, A.C. Watson, S.F. Glover, Development of integrated environmental control system designs for aircraft, Volume I-ECS Design, Technical Report AFFDL-TR-72-9, May 1972, Air Force Flight Dynamics Laboratory, Wright-Patterson Air Force Base, OH.
[10] F.P. Incropera, D.P. DeWitt, Fundamentals of Heat and Mass Transfer, third ed., Wiley, New York, 1990.
[11] W.M. Kays, A.L. London, Compact Heat Exchangers, third ed., McGraw-Hill, New York, 1984.
[12] A. Bejan, Heat Transfer, Wiley, New York, 1993.